Journal of
Synchrotron Radiation

ISSN 0909-0495

Received 26 August 2008
Accepted 19 December 2008

Polycapillary-optics-based micro-XANES and micro-EXAFS at a third-generation bending-magnet beamline

Geert Silversmit,[a]* Bart Vekemans,[a] Sergey Nikitenko,[b] Wim Bras,[b] Viktoria Czhech,[c] Gyula Zaray,[d] Imre Szaloki[e] and Laszlo Vincze[a]

[a]X-ray Microspectroscopy and Imaging Research Group (XMI), Department of Analytical Chemistry, Ghent University, Krijgslaan 281 S12, B-9000 Gent, Belgium, [b]Netherlands Organization for Scientific Research (NWO), DUBBLE@ESRF, BP 220, 38043 Grenoble Cedex 9, France, [c]Department of Plant Physiology, Eötvös Loránd University, 1117 Budapest, Pázmány Péter sétány 1/a, Budapest, Hungary, [d]Department of Inorganic and Analytical Chemistry, Eötvös Loránd University, 1117 Budapest, Pázmány Péter sétány 1/a, Budapest, Hungary, and [e]Institute of Experimental Physics, University of Debrecen, H-4026 Debrecen, Bem tér 18/a, Hungary. E-mail: geert.silversmit@ugent.be

A focusing system based on a polycapillary half-lens optic has been successfully tested for transmission and fluorescence μ-X-ray absorption spectroscopy at a third-generation bending-magnet beamline equipped with a non-fixed-exit Si(111) monochromator. The vertical positional variations of the X-ray beam owing to the use of a non-fixed-exit monochromator were shown to pose only a limited problem by using the polycapillary optic. The expected height variation for an EXAFS scan around the Fe *K*-edge is approximately 200 μm on the lens input side and this was reduced to ∼1 μm for the focused beam. Beam sizes (FWHM) of 12–16 μm, transmission efficiencies of 25–45% and intensity gain factors, compared with the non-focused beam, of about 2000 were obtained in the 7–14 keV energy range for an incoming beam of 0.5 × 2 mm (vertical × horizontal). As a practical application, an As *K*-edge μ-XANES study of cucumber root and hypocotyl was performed to determine the As oxidation state in the different plant parts and to identify a possible metabolic conversion by the plant.

Keywords: μ-XAS; μ-EXAFS; μ-XANES; polycapillary half-lens optic; non-fixed-exit monochromator; bending-magnet station.

1. Introduction

X-ray absorption spectroscopy (XAS) based experimental techniques such as XANES (X-ray absorption near-edge structure) and EXAFS (extended X-ray absorption fine structure) are widely used for structural characterization in a variety of disciplines and applications in order to extract information about the elemental local electronic and local structural configuration. Conventional XAS measurements make use of millimetre-sized X-ray beams which impose the condition that the samples should be homogeneous over the same length scale. When a microscopically inhomogeneous sample is measured with such beam dimensions, an average spectrum over the illuminated area is obtained in which the information on the spatial distribution is lost. To obtain spatially resolved spectra of microscopically heterogeneous samples, X-ray beams of micrometre dimensions are needed.

Focusing optics such as compound refractive lenses and Fresnel lenses are widely used but are less suitable for XAS owing to their achromatic focusing properties. To achieve a micro-focused beam, Kirkpatrick–Baez mirror systems are therefore sometimes incorporated in the beamline optics of undulator beamlines but are in fact less useful at bending-magnet beamlines since these mirror systems typically have relatively small acceptances which leaves a large amount of the available flux unused.

Glass polycapillaries are being used as focusing elements in, for instance, μ-XRF (X-ray fluorescence) experiments and can consequently present an alternative focusing optic for μ-XAS. This type of optic has an advantage owing to its relatively large acceptance (up to several millimetres horizontally and vertically), which allows the capturing of a relative large solid angle from the emitted bending-magnet spectrum. The transmission efficiency of the polycapillary half-lens is maximal for a parallel incoming beam; increasing the divergence of the incoming beam decreases the efficiency.

Although the use of polycapillary optics in μ-XANES has already been demonstrated (Vincze *et al.*, 2002; Proost *et al.*,

2003), the detailed characterization of its use in μ-EXAFS has, to our knowledge, not yet been reported. In this study a polycapillary half-lens is characterized as a focusing optic for transmission and fluorescence μ-EXAFS at the DUBBLE (BM26A, ESRF) beamline. The DUBBLE beamline is equipped with a non-fixed-exit double-crystal monochromator, delivering a monochromated X-ray beam of which the vertical position is X-ray energy dependent. As for a typical EXAFS spectrum, an energy range of about 1000 eV has to be scanned; this energy dependence of the vertical beam position is a major concern for μ-XAS applications. It is to be expected that the focusing properties of the polycapillary optic will eliminate or at least strongly reduce this vertical position shift. Obviously the vertical sample position could be adjusted to follow the X-ray beam, but this has the disadvantage that mechanical hysteresis could add to the systematic errors in position-sensitive measurements. Therefore it is important to accurately characterize the displacements of the X-ray beam over the sample as a function of energy. The suitability of the polycapillary as a focusing optic for μ-EXAFS is verified by recording spectra from several standards. Furthermore, as a practical application, an arsenic μ-XANES study of cucumber root and hypocotyl was performed.

2. Experimental

The experiments were performed at the DUBBLE beamline (BM26A) (Borsboom *et al.*, 1998) of the ESRF (Grenoble, France) during a uniform filling mode of the 6 GeV storage ring, typically yielding ring currents of 200 down to 160 mA during a synchrotron run. The DUBBLE XAS beamline receives a total of 2 mrad of the bending-magnet radiation fan (magnetic field strength B = 0.4 T, critical energy E_c = 9.6 keV). The horizontal and vertical divergences of the source are 103 μrad and 1.1 μrad, respectively. The beamline is equipped with a non-fixed-exit Si(111) double-crystal sagittal focusing monochromator. The higher harmonics of the primary energy were suppressed by a Si reflecting strip on a vertical focusing mirror after the monochromator. This mirror has a roughness of 1.5 Å r.m.s. and 1.5 μrad slope error and is placed under an angle of 2.8 mrad. The sagittal focusing capability of the monochromator was not used and the bending of the vertical focusing mirror was set as a flat mirror, in order to better match the acceptance of the polycapillary half-lens. The intensities of the incoming and transmitted X-ray beams were measured using ionization chambers (Oxford Instrument) and for fluorescence detection a liquid-nitrogen-cooled energy-dispersive nine-channel monolithic Ge detector (ORTEC, EG&G) (Derbyshire *et al.*, 1999) with XSPRESS electronics (Farrow *et al.*, 1995) was used.

Focusing was achieved using a large-acceptance polycapillary lens with an entrance diameter of 5 mm, an optic length of 50 mm, an exit diameter of 1.6 mm and a focal distance of 3.6 mm, manufactured by XOS (X-ray Optical Systems, USA), specifically designed for the beam characteristics of DUBBLE (*i.e.* with respect to source size/divergence, source–sample distance, bending-magnet energy range). Spectral data were recorded using a collimated incoming beam of size 0.5 × 2 mm [vertical (V) × horizontal (H)] with or without polycapillary focusing. The polycapillary was placed in between the first ionization chamber and the sample. An xyz coordinate system with its origin at the exit of the polycapillary optics, the x-axis along the X-ray beam propagation, the y-axis in the horizontal plane defined by the synchrotron orbit, and the z-axis in the vertical direction was used for further discussion and plotting of the results.

In order to determine the position of the focal plane and the vertical and horizontal beam sizes, a gold wire (thickness 180 μm) was scanned through the X-ray beam. Knife-edge scans were obtained by recording the transmitted X-ray intensity I_t with the second ionization chamber as a function of the scanning distance. The full width at half-maximum (FWHM) of a Gaussian fit to the derivative of the knife-edge scan (dI_t/dy) or (dI_t/dz) was taken as the vertical and horizontal FWHM beam sizes.

In addition to the knife-edge scans, X-ray images of the focused X-ray beam in the focal plane were taken using a SensiCam CCD (PCO Imaging, Germany; pixel size 0.67 μm). These images were used to determine the variations of the vertical and horizontal position of the focused beam as a function of X-ray energy.

The energy dependence of the polycapillary lens transmission efficiency (ε) was determined by monitoring the transmitted beam intensity (I_t) with and without polycapillary in the beam as a function of the X-ray beam energy. The ratio of the corresponding transmission signals normalized to their incoming intensities (I_0) gives the transmission efficiency.

The elemental detection limits for the fluorescence detection mode for this set-up were determined with the NIST SRM1577b (bovine liver) standard for a measuring time of 300 s and an excitation energy of 11.61 keV for the elements K to Zn.

The transmission EXAFS spectra of Ni, Cu and Zn foil and ZnO powder were recorded with and without the polycapillary focusing optics, in order to verify for any experimental artefacts that could be introduced by the use of the capillary optics. For the fluorescence detection mode, Zn K spectra of the NIST SRM1577b and Ni K spectra of the IRMM-301 standards were recorded.

All samples were measured in air under ambient conditions. The EXAFS data reduction and analysis were performed using the *XDAP* software (Vaarkamp *et al.*, 1995). The pre-edge background was subtracted using a modified Victoreen curve (Vaarkamp *et al.*, 1994) and the atomic background, μ_0, was subtracted using a cubic-spline routine (Cook & Sayers, 1981). The pre-edge background-subtracted spectra were normalized to the edge jump, which was taken as the value of the atomic background at 50 eV above the edge position.

With the characterized micro-focus set-up a study of the As speciation in different parts of cucumber plants was performed in order to investigate whether there is a metabolic conversion of arsenic during transport from the root towards

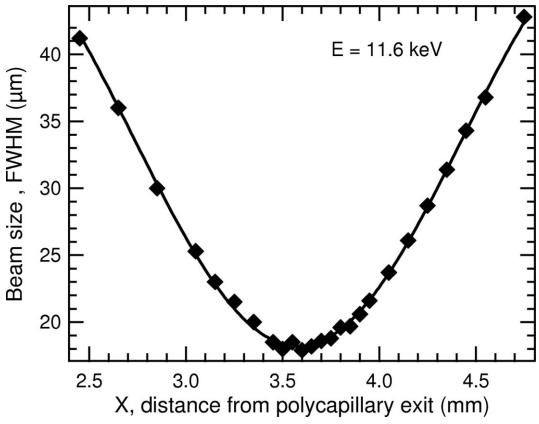

Figure 1
Measured vertical FWHM (μm) of the polycapillary focused microbeam as a function of the distance to the polycapillary exit window for an incident X-ray energy of 11.6 keV.

the stem of the plant. This is a subject with obvious relevance for environmental studies in contaminated soils.

3. Microbeam characterization

3.1. Beam size as a function of incident X-ray energy

In order to characterize the beam size and the depth of focus, the vertical FWHM of the focused beam at an X-ray energy of 11.6 keV as a function of the distance with respect to the exit window of the polycapillary device is given in Fig. 1.

The transmitted X-ray intensity *versus* distance obtained during vertical and horizontal knife-edge scans in the focal plane for an incident X-ray energy of 11.6 keV are given in Fig. 2; the corresponding derivative curves, $dI(z)/dz$, are also shown together with the resulting Gaussian fits. The FWHM of the Gaussian fit to the derivative curves is used to define the FWHM values of the focused beam.

In the focal plane an almost circular beam spot was observed even though the incoming beam had a rectangular shape of 0.5 × 2 mm (V × H) (see also §3.2). The variation of the vertical beam size as a function of X-ray energy is given in Fig. 3. For these measurements the beamline optics was optimized for an X-ray energy of 11.6 keV, and at each new energy value the height of the polycapillary was re-optimized towards a maximum transmitted signal. For an X-ray energy of 11.6 keV a smaller value compared with Fig. 1 is now obtained, owing to a re-alignment of the polycapillary.

3.2. Vertical and horizontal beam position

The Si(111) double-crystal monochromator at beamline BM26A is operated in a non-fixed-exit mode since the vertical offset mechanism of the second crystal has some design flaws. This implies that the height of the monochromated beam changes with energy. The vertical movement of the incoming beam on the polycapillary entrance can thus influence the position of the focused beam spot. X-ray images of the microbeam in the focal plane for different incoming X-ray energies ranging from 7 to 12 keV were taken; a selection is

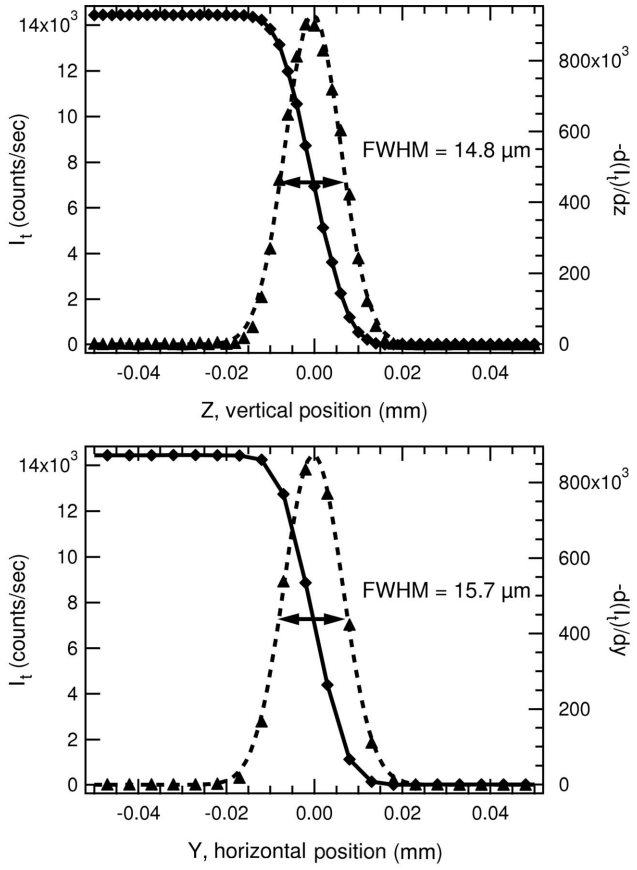

Figure 2
Vertical (top panel) and horizontal (bottom panel) knife-edge scans (solid lines and markers), together with the negative derivatives (markers) and the corresponding Gaussian fits (dashed line) for an incident X-ray energy of 11.6 keV.

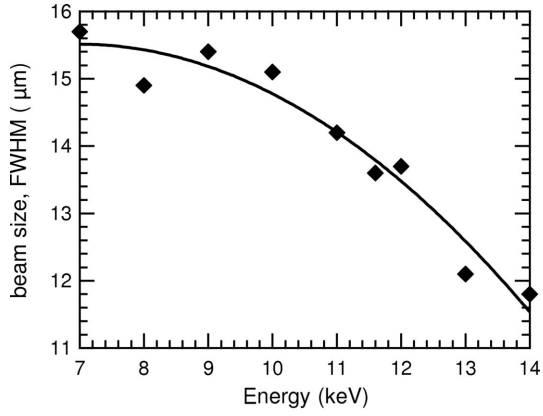

Figure 3
Measured vertical FWHM (μm) of the polycapillary focused microbeam as a function of incoming X-ray beam energy, determined by vertical Au knife-edge scans in the focal plane of the polycapillary.

shown in Fig. 4. Before taking these images, the beamline optics were optimized at 9.6 keV. In order to evaluate the influence of the energy-dependent vertical height of the incoming beam at the polycapillary entrance, no optimization of the optics (or position of the polycapillary) was performed at the other energies. This explains the drastic intensity drop at

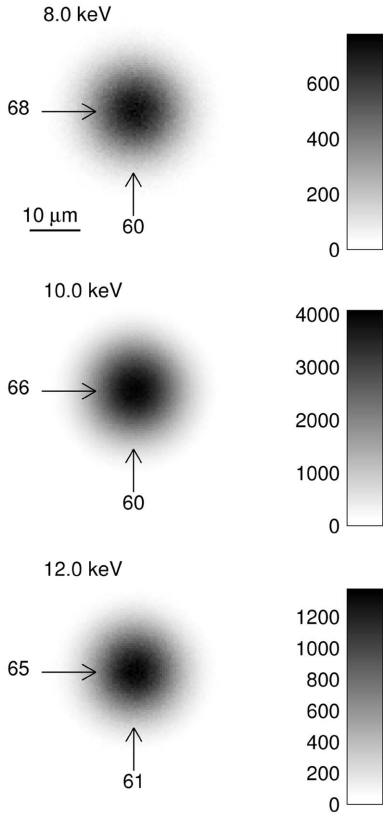

Figure 4
Two-dimensional X-ray images at the focal plane for different incoming X-ray energies. The arrows indicate the horizontal and vertical pixel position of the beam spot centre relative to the left lower corner. Incoming beam size: 0.5 × 2 mm (V × H).

the highest and lowest energies (all images were taken with identical settings for the X-ray camera). The horizontal and vertical pixel positions of the beam spot centre are indicated by the arrows in Fig. 4.

On the two-dimensional images from Fig. 4, vertical and horizontal beam profiles and positions were obtained by summing the total intensity in each data-row or column, respectively. In this way beam profiles were obtained that could be fitted with a Gaussian function on a constant background, illustrating the Gaussian intensity distribution of the focused beam. Fig. 5 shows the resulting vertical and horizontal profile positions as a function of incoming beam energy. From 8 keV on, the horizontal position is constant with energy, while a slight positional shift to the left is found between 7 and 8 keV. However, this shift is limited to about the size of one detector pixel (0.67 µm), so a constant horizontal beam position with energy (between 7 and 12 keV) can be assumed. The vertical position slightly changes with increasing energy. From 7 to 12 keV this shift was four pixels, or about 2.7 µm. For an EXAFS scan from 7–8 keV (worst case scenario in the energy range measured), this resulted in a shift of the vertical position of the focused beam of two pixels, ∼1.3 µm, which is only 10% of the focused beam size. However, the shift in the vertical position of the monochromated incoming beam for the same energy interval is about 190 µm.

3.3. Polycapillary transmission efficiency and gain factor

The energy dependence of the polycapillary lens transmission efficiency (ε) is shown in Fig. 6. The efficiency decreases as a function of energy from 45% to 25% in the 7–14 keV X-ray energy range. The flux-density or intensity gain factor (G) of the polycapillary lens can be calculated based on the measured transmission efficiency and the corresponding beam size as $G = \varepsilon S_{\rm input}/S_{\rm focal}$, where $S_{\rm input}$ and $S_{\rm focal}$ are the beam cross sections at the entrance of the polycapillary and in the focal plane. The intensity gains for an incoming beam size of 0.5 × 2 mm are shown in Fig. 6. Owing to the coupled variation of output beam flux and focused beam size, the flux-density gain varies only slightly in the energy range 7–14 keV, showing an average value of approximately 2000.

The estimated flux for the unfocused beam for the slit dimensions used [0.5 × 2 mm (V × H)] at 14 keV is $\sim 10^9$ photons s^{-1}. With the observed transmission efficiency of 20%, this results in an estimated flux of $\sim 2 \times 10^8$ photons s^{-1}.

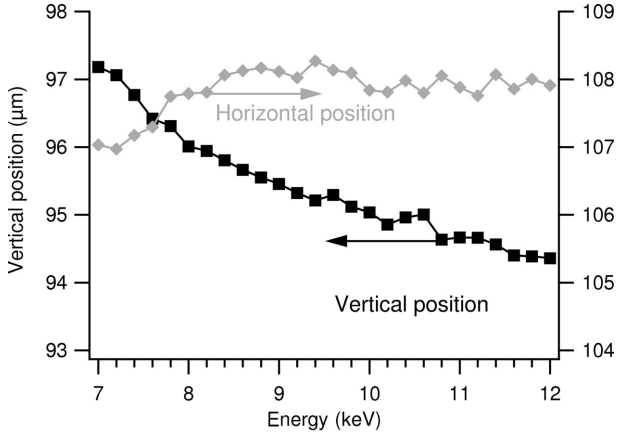

Figure 5
Vertical and horizontal beam positions in the focal plane as a function of incoming X-ray energy.

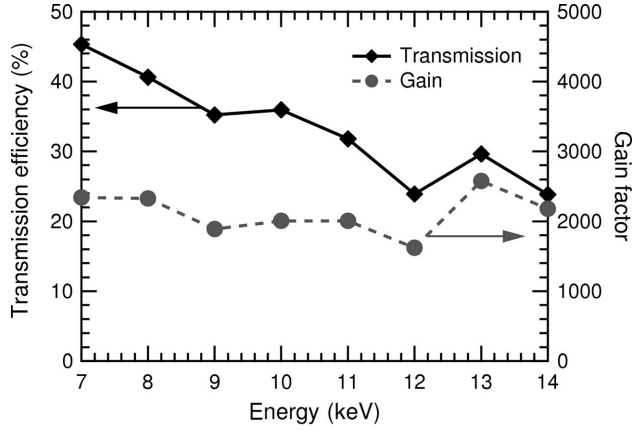

Figure 6
Polycapillary transmission efficiency and gain factor as a function of incoming X-ray energy.

3.4. Elemental detection limits of the fluorescence detection mode

The μ-XRF spectrum recorded with the central element of the monolithic energy-dispersive detector on a NIST SRM1577b (bovine liver) pellet excited with a focused beam of 11.61 keV using a measuring (real) time of 300 s is given in Fig. 7 together with the corresponding absolute and relative detection limits. For Zn (Z = 30) an absolute detection limit for the fluorescence emission of about 4 fg (0.2 p.p.m.) can be deduced.

3.5. Comparison with other typical μ-XAS bending-magnet stations

Dedicated μ-XAS stations are mostly constructed at insertion-device beamlines. Sagittal focusing by fixed-exit double-crystal monochromator and Kirkpatrick–Baez (KB) systems are often found at bending-magnet XAS stations. As an example of the first option we make a comparison with the FAME beamline, the French CRG at the ESRF. The FAME beamline uses dynamical sagittal horizontal focusing and a bent mirror after the monochromator for vertical focusing, resulting in beam sizes of about 150 × 200 μm (V × H) (Proux *et al.*, 2005), which is an order of magnitude larger compared with the beam dimensions obtained in this work using polycapillary optics.

Beamline 10.3.2 at the ALS is an example of a bending-magnet XAS station equipped with a KB mirror system. Using this focusing device, beam sizes of 5–20 μm are achieved (Marcus *et al.*, 2004). Preliminary experiments at the FAME beamline with a KB system resulted in beam sizes of 10 × 10 μm (Proux, 2008). As a general conclusion, the polycapillary optics used in our experiments resulted in beam sizes which are comparable with those obtained by KB systems installed at similar sources (*i.e.* bending magnet). Using polycapillary optics, when switching from one absorption edge to another (even when separated by several keV), only the height of the polycapillary lens needs to be re-adjusted. The strength of the polycapillary optics mainly lies in its ease of use in order to transform even a non-fixed-exit monochromator XAS station into a μ-XAS station.

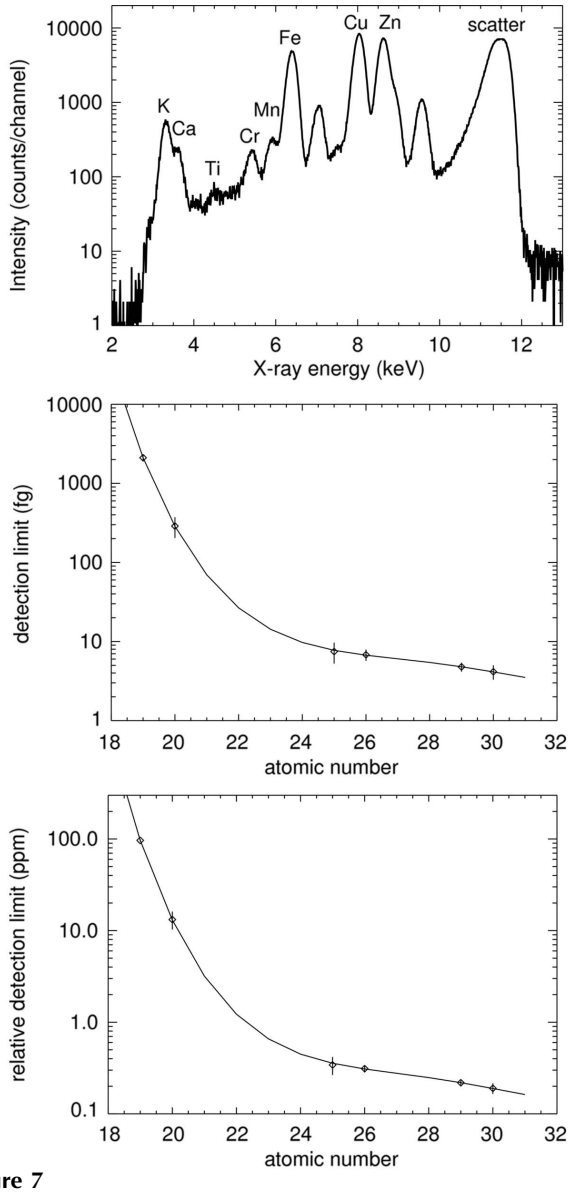

Figure 7
Top: μ-XRF spectrum taken of a SRM1577b (bovine liver) standard for an incoming X-ray energy of 11.61 keV and a real time of 300 s (the labels indicate the position of the $K\alpha$ fluorescence peak, and the broad peaks around 10–12 keV are the coherent and incoherent scatter contributions). Middle: corresponding absolute detection limits. Bottom: corresponding relative detection limits.

4. Comparative μ-EXAFS spectra of reference materials

4.1. Transmission μ-EXAFS spectra

Transmission XAS spectra of Ni foil, Cu foil, Zn foil and ZnO powder were recorded with and without a focusing polycapillary for an incoming beam size of 0.5 × 2 mm. The corresponding spectra are shown in Fig. 8. Generally, the spectra taken with the polycapillary focusing have different slopes in the pre- and post-edge region. This is due to the smoothly changing transmission efficiency of the polycapillary with X-ray energy. In order to correct the data for this effect, the transmission function, $\varepsilon(E)$, of the polycapillary was determined by scanning each energy range, with and without polycapillary (and without sample). As an example, the resulting energy-dependent transmission function for the Zn energy region is shown in Fig. 9. Note that the measured variation of transmission efficiency is mainly caused by the vertical movement (about 100 μm for the Zn XAS scan) of the incoming beam with respect to the optical axis of the polycapillary lens. With the observed dependence for $\varepsilon(E)$ it should be possible to correct for the variation in the transmission efficiency. Let $\mu x' = \ln(I_0/I_t')$ be the measured absorption coefficient for the focused case, with I_0 the incoming intensity and I_t' the transmitted X-ray intensity. If the same spectrum would have been recorded without focusing, the same I_0 would have been measured, but a different transmitted intensity I_t would have been obtained, with $I_t' = I_t\varepsilon(E)$. So a corrected absorption, $\mu x_{cor} = \ln[I_0\varepsilon(E)/I_t']$, can be calculated. The resulting corrected absorption

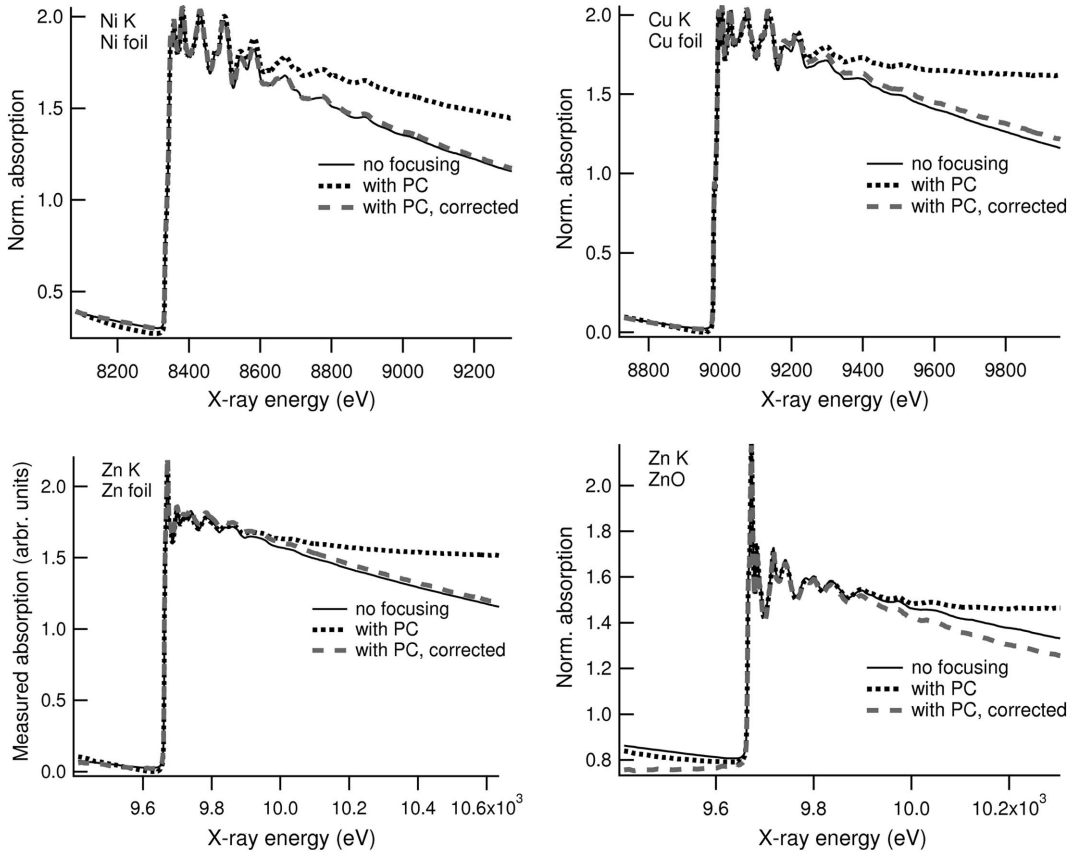

Figure 8
Transmission XAS spectra for Ni foil, Cu foil, Zn foil and ZnO powder recorded with and without polycapillary (PC) focusing; focused spectra corrected for the polycapillary transmission function are also given.

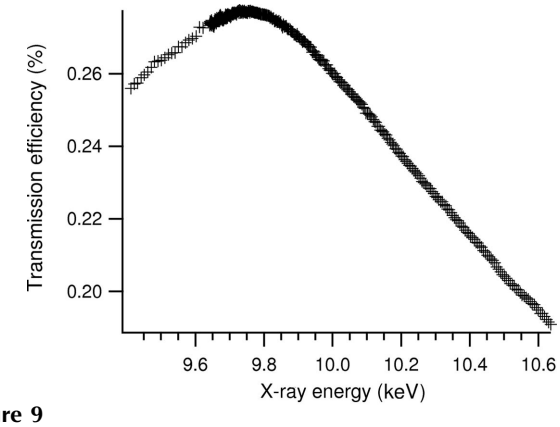

Figure 9
Transmission efficiency of the polycapillary lens as a function of X-ray energy for the energy range scanned for the XAS transmission spectra of the Zn foil from Fig. 8.

spectra are also given in Fig. 8; the slopes of the pre-edge and post-edge regions are now very close to the transmission spectrum recorded without focusing. The pre-edge region for the ZnO spectrum looks overcorrected owing to a large time difference between the recording of this spectrum and the recording of the polycapillary transmission function.

The transmission $k^3\chi(k)$ EXAFS signals and corresponding Fourier transforms $\{\mathrm{FT}[k^3\chi(k)]\}$ for the unfocused and focused cases are given in Fig. 10, together with the spectra corrected for the polycapillary transmission. The spectra are very similar compared with the unfocused spectra for all samples, except for the Zn foil. The reason for this is not clear, but as the spectra for ZnO are similar this points most likely towards a sample problem for the Zn foil. There is no need to correct the EXAFS spectra for the polycapillary transmission function, as for all samples the corrected EXAFS spectra and Fourier transforms are identical to the not-corrected polycapillary spectra.

The XAS spectra with the polycapillary focusing were recorded with the same time settings as in the unfocused case. As the intensity is only 20–30% compared with the unfocused case, this results in a decreased data quality for spectra recorded with the polycapillary.

4.2. Fluorescence μ-EXAFS spectra

The NIST standard reference material SRM1577b (bovine liver) is a biological reference powder with a Zn concentration of 127 μg g^{-1}. Zn *K* XAS spectra were taken on a pressed disc of 18.7 mg with a diameter of 6.5 mm. With a beam spot FWHM of about 15 μm at the Zn *K* edge (∼9.6 keV), this results in a probed Zn mass of about 3 pg (if no self absorption is assumed, so the real probed mass will be lower). The Zn *K* $k^1\chi(k)$ EXAFS spectra and corresponding FT$[k^2\chi(k)]$ signals of the NIST SRM1577b pellet recorded in fluorescence mode

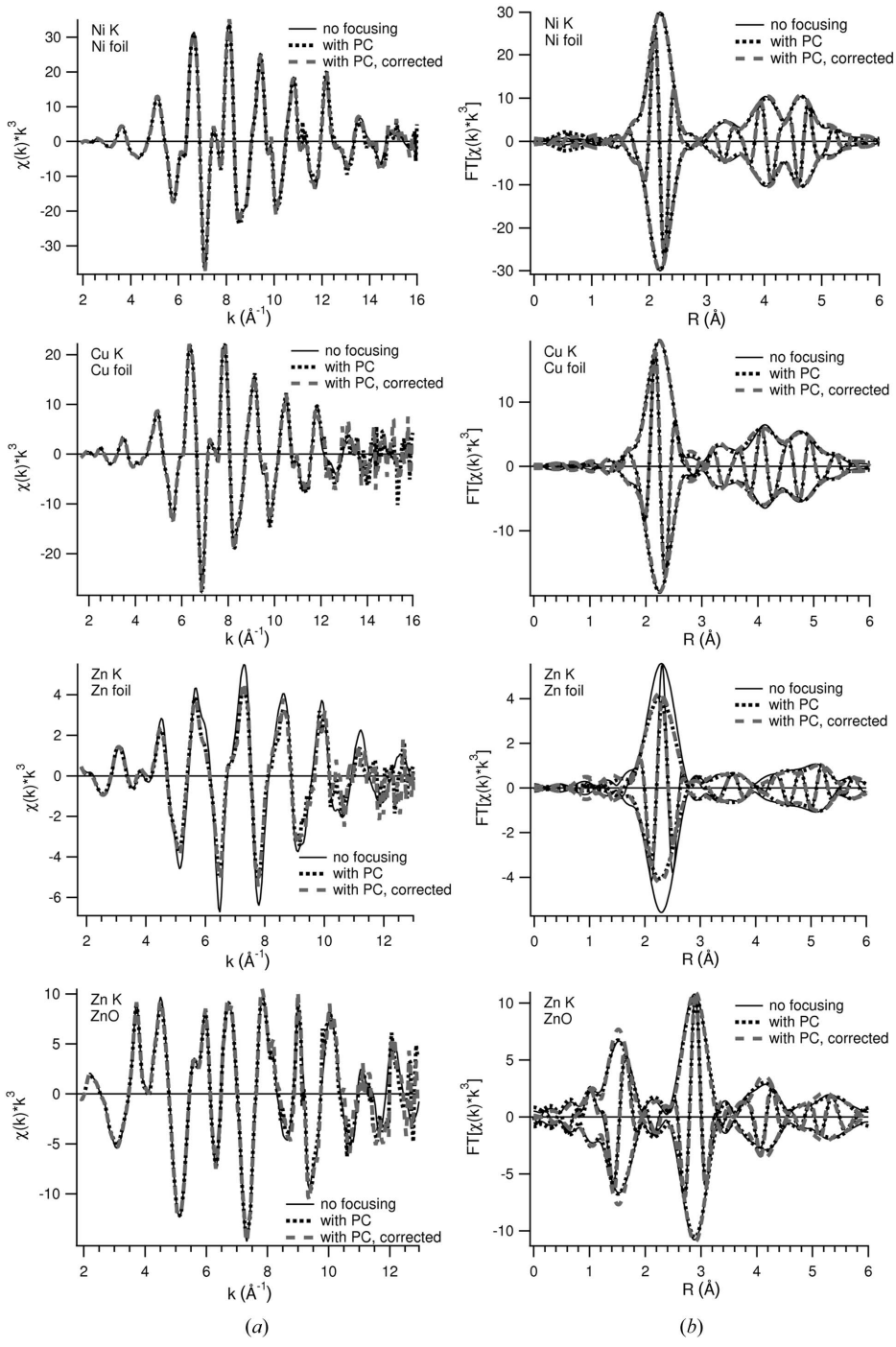

Figure 10
Transmission $k^3\chi(k)$ (*a*) and FT[$k^3\chi(k)$] spectra (*b*) for Ni foil, Cu foil, Zn foil and ZnO recorded without polycapillary (PC) focusing compared with the spectrum taken with focusing and the focused spectrum corrected for the polycapillary transmission efficiency (Ni: Δk = 2.8–14.7 Å^{-1}; Cu: Δk = 2.12–13.62 Å^{-1}; Zn foil: Δk = 3.4–12.2 Å^{-1}; ZnO: Δk = 2.5–12.4 Å^{-1}).

with and without the focusing polycapillary are given in Fig. 11. Both spectra are identical, and no effect of the polycapillary is present on the EXAFS spectra in the fluorescence mode.

The IRMM-301 standard is a micro-structured reference material consisting of permalloy (81% Ni, 19% Fe) strip patterns on a silicon substrate. The strip patterns are between 2 and 100 µm wide and have a height of 0.5 µm. Ni *K* fluorescence XAS spectra were taken on a horizontal strip with a width of about 20 µm. At the Ni *K* edge (8333 eV) the focused beam has a FWHM of about 15.5 µm (see Fig. 3), and the total Ni mass in the illuminated volume is about 670 pg (permalloy has a face-centred-cubic crystal structure with a = 0.355 nm). As we did not have the fluorescence spectrum of the fully illuminated sample, the XAS spectra are compared with the transmission spectrum from a Ni foil {see Fig. 12 for the normalized absorption spectra and Fig. 13 for the $k^1\chi(k)$ and the FT[$k^3\chi(k)$] spectra}. The spectra are identical in shape, but compared with the Ni foil a lower intensity in the EXAFS spectrum and Fourier transform for the µ-XAS spectra on the strip is observed. The fluorescence EXAFS spectra were corrected for self-absorption using the Booth–Bridges method (Booth & Bridges, 2005) in the *ATHENA* package (Ravel & Newville, 2005) and are also given in Fig. 13. The observed difference in amplitude cannot be ascribed to self-absorption in the fluorescence detection. Based on the similarity between the focused and not focused transmission spectra and the fluorescence spectrum on the NIST SRM1577b, we conclude that the difference in amplitude in the IRMM-301 EXAFS spectra is due to comparing different samples and different detection modes.

5. Practical study: As *K* XANES of cucumber plant parts

The presence of arsenic in the soil and in surface water is an important environmental problem for humans, animals and plants. The As(III) compound for example has the ability to inhibit ATP production and results in the cessation of organ functions, especially in the case of acute arsenic poisoning. Arsenic disturbs the biochemical processes in plants after uptake and can lead to leaf dieback from the tip, fruit of poor quality and development of sterile flowers resulting in low grain yields.

After uptake by the plant the oxidation state of As can be changed *via* metabolic conversion and, since the toxicity of arsenic depends on its oxidation state and coordination

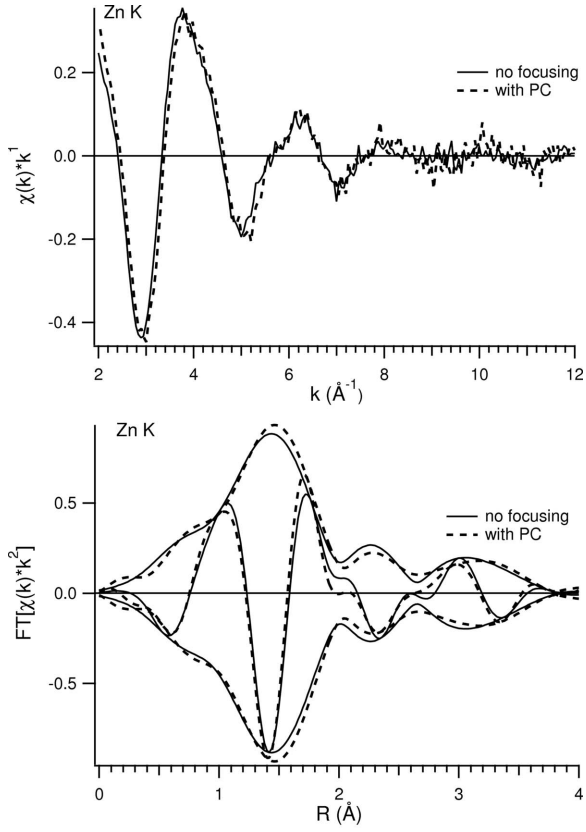

Figure 11
Zn *K* fluorescence $k^1\chi(k)$ (top) and FT[$k^2\chi(k)$] spectra (bottom) from a NIST SRM1577b (bovine liver) pellet recorded with polycapillary (PC) focusing compared with the spectrum taken without focusing (PC focusing, Δk = 2.47–8.58 Å^{-1}; no focusing, Δk = 2.41–8.53 Å^{-1}).

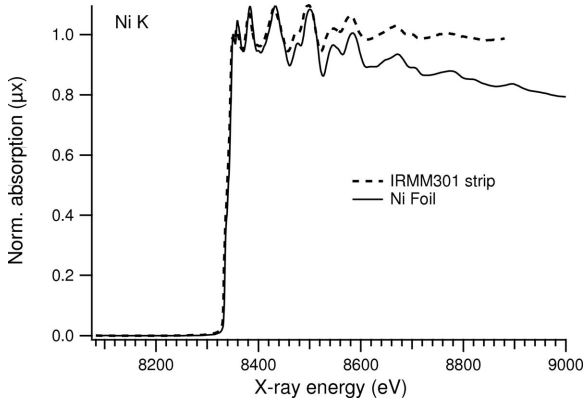

Figure 12
Normalized Ni *K* fluorescence XAS spectra of a horizontal 20 μm-wide permalloy strip of the IRMM-301 reference standard recorded with polycapillary focusing, and the transmission spectrum on a Ni foil without focusing.

[As(III) is the most toxic variant of the As compounds for instance], it is necessary to know the As oxidation state in the different plant parts. Stem hypocotyl and root parts of cucumber plants treated with As(V) in Hoagland nutrient solutions (Ca, K, Mg, Fe, B, Mn, Zn, Cu, Mo) were studied *in vivo* in order to study the changes in the As oxidation state during transport from the roots to the stem of the cucumber plant.

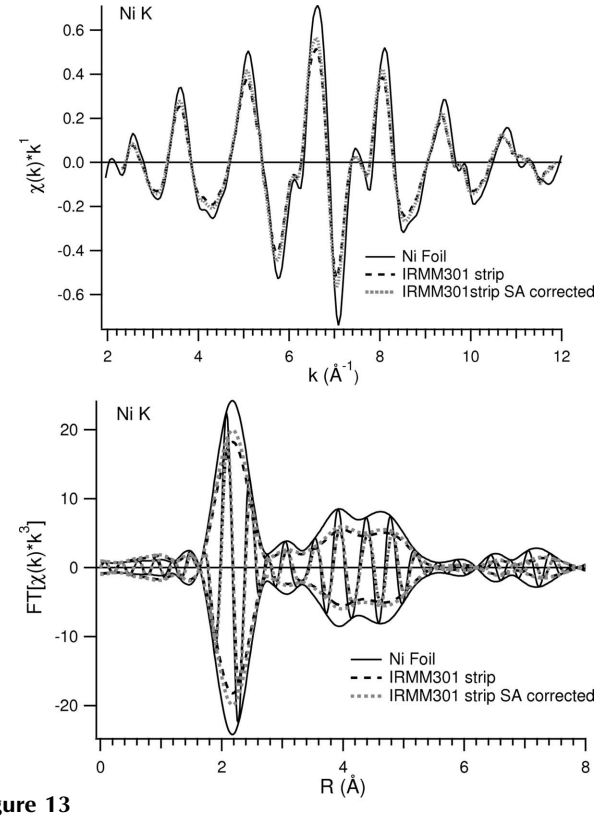

Figure 13
Ni *K* fluorescence EXAFS spectra of a horizontal 20 μm-wide permalloy strip of the IRMM-301 reference standard recorded with polycapillary focusing, and the transmission spectrum on a Ni foil without focusing; $k^1\chi(k)$ spectra (top) and FT[$k^3\chi(k)$] (bottom) (IRMM: Δk = 2.40–11.31 Å^{-1}; Ni foil: Δk = 2.42–11.36 Å^{-1}). The EXAFS spectra corrected for self-absorption (SA) are also added.

The As *K* XANES spectrum taken of the root without focusing is shown in Fig. 14 (top, black solid line) and compared with As(III) and As(V) spectra obtained from reference solutions. The main contribution in the root spectrum is As(V) with a shoulder at lower energy. This minor contribution is situated below the As(III) position and can be addressed to As(II) or As(III) compounds in which arsenic is coordinated to sulfur such as in As(II)S (Webb *et al.*, 2003; Liu *et al.*, 2008; Kwong *et al.*, 2007), $As(III)_2S_3$ (Liu *et al.*, 2008; Kwong *et al.*, 2007) and $As(III)Glu_3$ (As bound to S in glutathione) (Pickering *et al.*, 2000; Foust *et al.*, 2004; Gault *et al.*, 2008). We will further refer to this compound as As-S throughout this manuscript

Several spectra with the focused beam were taken. The first, last and an intermediate spectrum are shown in Fig. 14 (top). In this sequence the As-S contribution disappears with time and the main edge shifts towards higher energy. The position of the As(V) absorption edge and the maximum of the main absorption peak shifts by less than 1 eV towards higher energy. Such a small shift cannot be assigned to a change in the As(V) oxidation state. Generally, a small shift in absorption edge can be induced by a change in coordination. So the difference in the energy position of the two peaks (and absorption edges) can be due to different As coordinations with the same As(V) oxidation state. Indeed, Pickering *et al.*

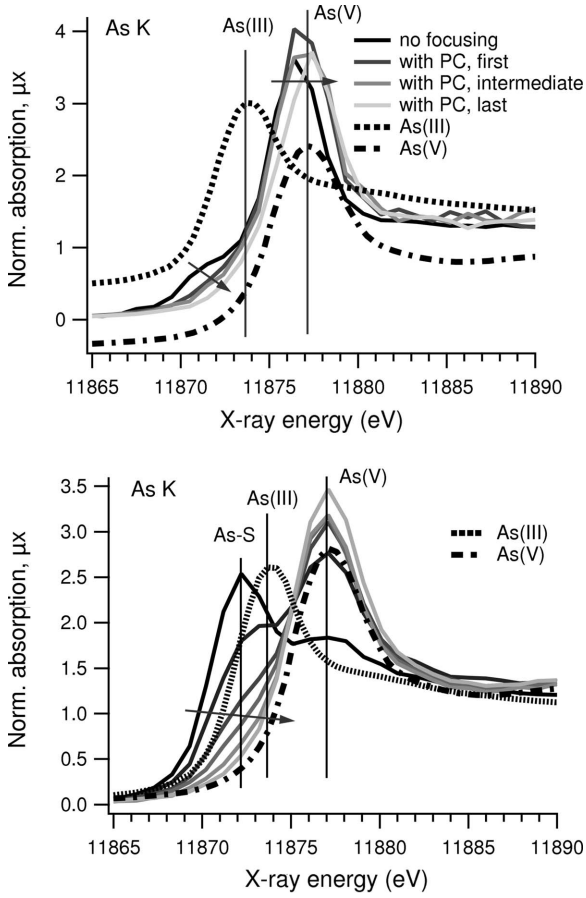

Figure 14
As *K* fluorescence XANES spectra of a cucumber root (top) and hypocotyl stem (bottom), together with As(III) and As(V) reference spectra.

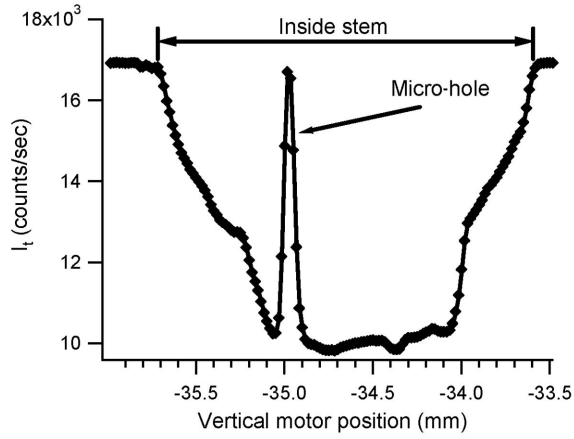

Figure 15
Transmission ionization chamber signal for a vertical scan over a cucumber hypocotyl stem, showing the micro-hole drilled by the focused microbeam.

(2000) report As *K* XANES spectra of aqueous solutions of arsenite [As(III)] and arsenate [As(V)] at two different pH values. Higher pH values result in a small shift (<1 eV) of the absorption edge towards lower energy.

The plant nutrition solution contained As(V); a small part of the arsenic in the roots is As-S, owing to metabolic conversion in the cucumber root. Under influence of the X-ray beam the arsenic fully oxidizes towards As(V). Besides the oxidation a change in the As(V) coordination occurs under the irradiation of the focused beam.

Spectra with the focused beam of the hypocotyl stem could not be obtained. The radiation damage on this part of the plant was so high that a micro-hole was burned through the stem (see Fig. 15). Therefore only spectra without focusing could be recorded of the stem. The sequence of spectra as a function of time is given in Fig. 14 (bottom). The first scan shows a major peak at an energy position below As(III) which can again be assigned to As-S, a second contribution of As(V) and a possible not-resolved As(III) contribution. The second spectrum has a major As(V) contribution and a lower As(III) contribution [and a minor As-S contribution as the edge position is still lower than for the As(III) reference]. From the third spectrum on, the scans rapidly converge to the spectrum of the As(V) reference solution [with a minor and rapidly decreasing As(III) contribution]. As the sample is already irradiated during alignment, the As oxidation state in the fresh stem can already be influenced by the X-ray beam before the first scan was recorded. From this, however, it cannot be concluded that only As-S was present in the fresh not irradiated stem, although it is the main oxidation state present in the stem. After uptake of the As(V) from the solution by the roots, the arsenic is converted to As-S compounds during transport to the stem.

A possible solution to the problem of radiation damage on these samples would be to cool the samples to cryogenic temperatures in order to limit the mobility of the free radicals that are supposedly the main cause of radiation damage. So far we have not attempted this due to the fact that the working distance of the polycapillaries is limited to some millimetres and the cryogenic jet of conventional cooling devices will also affect the polycapillary itself. Notwithstanding the problems that we have encountered with these biological samples, the use of polycapillaries as focusing elements in EXAFS experiments has been proven to be possible and very promising for the studies of more radiation-resistant materials.

6. Conclusions

A μ-XAS set-up based on a polycapillary half-lens as a focusing optic element has been characterized and successfully tested for transmission and fluorescence μ-EXAFS at the DUBBLE (BM26A, ESRF) beamline, a bending-magnet XAS station equipped with a non-fixed-exit double-crystal monochromator. The polycapillary lens was tested in the 7–14 keV X-ray energy range and provided beam sizes (FWHM) of 12 μm (14 keV) to 16 μm (7 keV). An energy-dependent transmission efficiency of 25–45% was observed and the overall gain factor was about 2000. The energy-dependent vertical beam position owing to the non-fixed-exit monochromator is strongly suppressed by the focusing of the polycapillary.

The suitability for using this optic in μ-EXAFS is demonstrated with comparative spectra obtained from several reference compounds and standards. Although the absorption spectra can be corrected for the smoothly changing polycapillary transmission function as a function of X-ray energy, the transmission function does not generally alter the EXAFS spectra, making the correction not mandatory for the EXAFS analysis.

As a practical application, As *K* μ-XANES spectra of cucumber plants treated with As(V) were recorded. These spectra showed that the As(V) portion taken up by the roots is converted to As-S [As(II) or As(III)] during transport towards the stem of the plant but it also shows that the local X-ray doses can exceed the threshold for the occurrence of radiation damage.

We kindly thank A. Snigirev for providing the high-resolution X-ray camera, and the staff of DUBBLE for technical support. Dr G. Silversmit is supported by a postdoctoral fellowship from the Research Foundation-Flanders (FWO-Vlaanderen, Belgium). This research was performed as part of the Interuniversity Attraction Poles (IAP6) programme financed by the Belgian Government. FWO-NWO are thanked for making the beam time on the DUBBLE beamline available.

References

Booth, C. H. & Bridges, F. (2005). *Phys. Scr.* T**115**, 202–204.
Borsboom, M., Bras, W., Cerjak, I., Detollenaere, D., Glastra van Loon, D., Goedtkindt, P., Konijnenburg, M., Lassing, P., Levine, Y. K., Munneke, B., Oversluizen, M., van Tol, R. & Vlieg, E. (1998). *J. Synchrotron Rad.* **5**, 518–520.
Cook, J. W. Jr & Sayers, D. E. (1981). *J. Appl. Phys.* **52**, 5024–5031.
Derbyshire, G., Cheung, K.-C., Sangsingkeow, P. & Hasnain, S. S. (1999). *J. Synchrotron Rad.* **6**, 62–63.
Farrow, R., Derbyshire, G. E., Dobson, B. R., Dent, A. J., Bogg, D., Headspith, J., Lawton, R., Martini, M. & Buxton, K. (1995). *Nucl. Instrum. Methods Phys. Res. B*, **97**, 567–571.
Foust, R. D., Mohapatra, P., Compton-O'Brien, A.-M. & Reifel, J. (2004). *Appl. Geochem.* **19**, 251–255.
Gault, A. G., Rowland, H. A. L., Charnock, J. M., Wogelius, R. A., Gomez-Morilla, I., Vong, S., Leng, M., Samreth, S., Sampson, M. L. & Polya, D. A. (2008). *Sci. Total Environ.* **393**, 168–176.
Kwong, Y. T. J., Beauchemin, S., Hossain, M. F. & Gould, W. D. (2007). *J. Geochem. Explor.* **92**, 133–150.
Liu, S., Jing, C. & Meng, X. (2008). *Sci. Total Environ.* **392**, 137–144.
Marcus, M. A., MacDowell, A. A., Celestre, R., Manceau, A., Miller, T., Padmore, H. A. & Sublett, R. E. (2004). *J. Synchrotron Rad.* **11**, 239–247.
Pickering, I. J., Prince, R. C., George, M. J., Smith, R. D., George, G. N. & Salt, D. E. (2000). *Plant Physiol.* **122**, 1171–1177.
Proost, K., Vincze, L., Janssens, K., Gao, N., Bulska, E., Schreiner, M. & Falkenberg, G. (2003). *X-ray Spectrom.* **32**, 215–222.
Proux, O. (2008). Personal communication.
Proux, O., Biquard, X., Lahera, E., Menthonnex, J.-J., Prat, A., Ulrich, O., Soldo, Y., Trévisson, P., Kapoujyan, G., Perroux, G., Taunier, P., Grand, D., Jeantet, P., Deleglize, M., Roux, J.-P. & Hazemann, J. L. (2005). *Phys. Scr.* T**115**, 970–973.
Ravel, B. & Newville, M. (2005). *J. Synchrotron Rad.* **12**, 537–541.
Vaarkamp, M., Dring, I., Oldman, R. J., Stern, E. A. & Koningsberger, D. C. (1994). *Phys. Rev. B*, **50**, 7872–7883.
Vaarkamp, M., Linders, J. C. & Koningsberger, D. C. (1995). *Physica B*, **208–209**, 159–160.
Vincze, L., Wei, F., Proost, K., Vekemans, B., Janssens, K., He, Y., Yan, Y. & Falkenberg, G. (2002). *J. Anal. Atom. Spectrom.* **17**, 177–182.
Webb, S. M., Gaillard, J.-F., Ma, L. Q. & Tu, C. (2003). *Environ. Sci. Technol.* **37**, 754–760.